Int. J. New. Chem., 2022, Vol. 9, Issue 4, pp. 351-382.

International Journal of New Chemistry

Published online 2022 in http://www.ijnc.ir/.

Open Access

Print ISSN: 2645-7237

Online ISSN: 2383-188x

Original Research Article

2D-QSAR, 3D-QSAR, molecular docking, and molecular dynamics simulations in the probe of novel type I diabetes treatment

Emmanuel Israel Edache[1,2*], Adamu Uzairu[2], Paul Andrew Mamza[2] and Gideon Adamu Shallangwa[2]

[1] Department of Pure and Applied Chemistry, University of Maiduguri, Borno State, Nigeria.

[2]Department of Chemistry, Ahmadu Bello University, P.M.B. 1044, Zaria, Nigeria.

Received: 2022-10-01 *Accepted: 2022-12-15* *Published: 2022-12-22*

ABSTRACT

The 2D and 3D QSAR of 30 compounds with type 1 diabetes inhibitors has been studied by using semi-empirical methods. The parametrization (PM6) method is employed as the basic set to optimize the derivatives using Spartan 14 and PaDEL v2.20 are used to calculate the chemical descriptors. To obtain a reliable QSAR model, the data set using the Kennard-Stone method to divide the derivatives into training set and test set comprising 21 and 9 compounds, respectively. An optimal model for the training set with significant statistical quality was established. The same model was further applied to the test set pIC50 of the 9 compounds. In the 2D-QSAR study, the MLR analysis produced 2 models, where the best one is model 2 with SEE = 0.3227; r^2 = 0.7409; r^2 adjusted = 0.6952; F = 16.20625. In the 3D-QSAR study, Atom-based fashion and pharmacophore-based fashion alignment were used. The results showed that CoMFA (uvepls) (q2 = 0.6897; r2 = 0.9999) have good stability and predictability. The internal validation indicated that CoMFA (uvepls) MIFs possess good predictive power than COMFA (ffdsel). The molecular docking study showed three (3) conventional hydrogen bonds with Arg97, Glu63, and Tyr159. Two carbon-hydrogen bonds with Ala69 and His70. MD simulation (1ns) analysis on the docked compound 17 assisted in the further exploration of the binding interactions. Some crucial interactions like pi-pi-T-shaped and amide-pi-stacked were identified. Hydrogen bond interactions with Arg97, Tyr7, and Trp167, respectively, bind more closely to the ligand. These results can offer useful insights for future investigational type 1 diabetes inhibitors.

Keywords: Type 1 diabetes, 2D-3D QSAR, Open3DALIGN, Open3DQSAR, Docking simulation, Molecular Dynamic simulations.

***Corresponding Author: Tel: +2348066776802**
E-mail: edacheson2004@gmail.com

Introduction

Diabetes is a major public health issue that is rapidly spreading around the world [1]. Type 1 diabetes (also known as insulin-dependent diabetes or juvenile diabetes) is most commonly diagnosed in adolescents, teens, and young adults, but it can strike anyone at any age [2]. Type 1 diabetes is believed to be caused by an autoimmune reaction (when the body accidentally attacks itself) that kills the insulin-producing beta cells in the pancreas [3]. Insulin is a hormone that aids the entry of blood sugar into cells where it can be used for energy (or body buildup). Blood sugar cannot enter cells without insulin, and it accumulates in the bloodstream. High blood sugar harms the body and contributes to many of the signs and problems associated with diabetes. Early signs and symptoms include extreme thirst and excessive urination. More serious symptoms, such as fast, deep breathing, dry skin, and mouth, flushed face, fruity-smelling breath, headache, muscle weakness or aches, being very tired, nausea and vomiting, and stomach pain, can occur quickly if left untreated [2]. Hypoglycemia can be caused by too much insulin, and diabetic ketoacidosis can be caused by too little insulin. There is a diabetes epidemic going on right now. Diabetes prevalence was 8.0 percent in 2007 and is projected to increase to 7.3 percent by 2025, according to the International Diabetes Federation. Diabetes currently affects 246 million people (46 percent of whom are between the ages of 40 and 59), with the figure projected to increase to 380 million by 2025 (www.diabetesatlas.org). As per the fifth edition of the world diabetes atlas published by the International Diabetes Federation (IDF) in 2011, the total adult population in the age range of 20-79 years is estimated to be 3-4 billion in 2011, with millions of people living with diabetes [5]. Research shows that there is a significant increase in the prevalence of diabetes, from 2013 to 2018 which was 6.9% to 8.5% [6]. World health organization (WHO) anticipated that 347 million

individuals have blood sugar (diabetes), which is anticipated to be the seventh driving reason of deaths by 2030 [7], while Wild and his co-worker projected approximately 400 million cases in 2030 contrasted with 171 million in 2000 [8, 9]. Drugs like metformin, SGLT2 inhibitors, and GLP1 receptor agonists have been prescribed to people with diabetes, unfortunately, these drugs have adverse effects such as heart failure, higher risk of urinary, genital infections, ketoacidosis, and gastrointestinal problem (such as nausea and a loss of appetite) on individuals [2]. However, all these drugs give only temporary relief and are associated with a lot of side effects. Apart from these side effects, reported compounds are less potent. Hence, great opportunities still present for computer-aided drug design in search of potent drugs and accordingly to obtain insights into the active site of an enzyme. Therefore, there is an urgent need to develop effective and safer alternative drugs for the prevention and treatment of type 1 diabetes. Lately, computer-aided drug design has been utilized to model not only biological activities,[10] but also chemical properties, docking, molecular simulations [11], and ADMET condition [12]. As a result, it is important to develop a 2D, 3D-QSAR and docking model for predicting the behavior of modeled compounds before their synthesis. A effective QSAR model not only aids in the understanding of relationships between structural features and biological activity of any class of compounds, but it also provides researchers with a comprehensive analysis of the lead compounds to be used in subsequent studies [13]. Furthermore, recognizing the mechanism of ligand-receptor interactions is critical in the development of drugs, and the molecular docking simulation approach is a good way to do so [11]. Molecular docking simulation is a statistical method for predicting the ability of active site residues to bind to particular receptor groups and evaluating the strength of interaction [12]. The drug research industry uses molecular docking to test the coupling of small molecules (inhibitors) to receptors (macromolecules) [13]. Using all-atom molecular dynamics (MD) simulations, confirm

the efficiency of hits bound to the binding site and construct the complex to determine the behavior of leads in complex structures [14, 15]. MD simulation is a sophisticated technique for observing the dynamics of all atoms in a system by simulating the action of molecules in a complex structure [12].

Materials and Methods

For 2D/3D quantitative structure-activity relationship (QSAR), molecular docking, molecular dynamics simulations studies a series of 30 compounds with their IC_{50} (mM) were collected from a lately published study [2]. To minimize the skewness of the data collection, *in vitro* biochemical activities (IC_{50} (mM)) were translated into molar (M) range and then into corresponding pIC_{50} values (i.e. pIC_{50} is the negative logarithm of IC_{50} (pIC_{50} = -log IC_{50})). These compounds' smile structures and their Pubchem CID numbers, experimental, and pIC_{50} are presented in Table 1. The molecular structure was sketched using MavinView software, and then, were minimized/optimized by the semi-empirical PM6 method included in the Spartan'14 v1.1.4 program. Thereafter, the molecular descriptors calculated with PaDEL-Descriptor [16] were subsequently subjected to variable reduction using a Data Pre-Treatment Tool (V-WSP Tool) [17]. Using the Kennard-Stone (http://dtclab.webs.com/software-tools) methodology, the data set was divided into two groups: training and test sets. The training set, which consisted of 21 (70%) molecules, was used for model production, while the test set, which consisted of 9 (30%) molecules, was used to avoid overtraining and assess the predictive power of the generated model using the best subset selection (BSS) multiple linear regression (MLR).

Table 1. Smile structure, PubChem CID number, bioactivity, and docking results of the studied compounds

S/N	Smile Structure	CID	IC_{50} value (mM)	pIC_{50}	Docking Score
1	CCN1N=C(N=C2C(=O)N(C)C(=O)N=C12)c3ccccc3	647501	10.421	4.9821	-7.3
2	OC(=O)[C@@H]1Nc2:c(O):c:c:c:c:2[C@H]3C=CC[C@@H]13	654089	8.35	5.0783	-7.5
3	[O-][n+]1:o:n:c(C(=O)c2:c:c:c:s:2):c:1C(=O)c3:c:c:c:s:3	573747	1.24	5.9066	-6.8
4	OC(=O)CCCNc1:c:c(N2CCC3(CC2)OCCO3):c4:n:o:c5c6:c:c:c:c:c:6C(=O)c:1:c:4:5	3239469	61.947	4.2080	-8.8
5	CN1N=CN=C2C(=O)N(C)C(=O)N=C12	66541	1.24	5.9066	-6.3
6	CN1N=C(C)N=C2C(=O)N(C)C(=O)N=C12	460747	1.24	5.9066	-6.8
7	CC(C)(CS(=O)(=O)[O-])NC(=O)CC[N+](C)(C)CCO	1973720	4.076	5.3898	-4.9
8	OC(=O)CCCN1C(=S)S\C(=C\c2:o:c(:c:c:2)c3:n:c4:c:c:c:c:c:4:s:3)\C1=O	2012947	4.773	5.3212	-8.1
9	CC(=O)c1:c:c:c2N[C@H]([C@@H]3C[C@@H](Sc4:c:c:c:c:c:4[N+](=O)[O-])[C@H](Cl)[C@H]3c:2:c:1)C(=O)O	3116376	57.855	4.2377	-8.4
10	CCc1:n:n:c(NS(=O)(=O)c2:c:c:c(NC(=O)C3=Cc4:c:c:c:c(CC=C):c:4OC3=O):c:c:2):s:1	1714876	9.427	5.0256	-9
11	COc1:c:c:c:c(\C=N/NC(=O)c2:c:c3:c:c(:c:c:c:3:s:2)[N+](=O)[O-]):c:1O	86261486	13.108	4.8825	-7.6
12	CCOc1:c:c(\C=C\2/NC(=O)NC2=O):c:c(Br):c:1OCc3:c:c:c(:c:c:3)C(=O)O	1334608	2.394	5.6209	-8.2
13	Oc1:c:c:c(:c:c:1)C(=O)N\N=C\c2:c:c:c(OCC(=O)Nc3:c:c:c:c(:c:3)[N+](=O)[O-]):c:c:2	9564046	37.577	4.4251	-7.5
14	CCOc1:c:c(\C=N/NC(=O)c2:c:c:c(:c:c:2)c3:c:s:c(Nc4:c:c:c(C):c:c:4):n:3):c:c:c:1OCC(=O)O	9595043	4.683	5.3295	-7.5

15	COc1:c:c:c(:c:c:1)\N=C\2/S\C(=C\c3:c:c:c(OCC(=O)O):c:c:3)\C(=O)N2CCc4:c:[nH]:c5:c:c:c:c:c:4:5	5995173	1.24	5.9066	-8.3
16	CCOC(=O)c1:s:c2N=C3N(C=C(C=C3SCCC(=O)O)C(=O)c4:c:c(OC):c:c:c:4O)C(=O)c:2:c:1C	2545524	2.02	5.6946	-7.2
17	Cc1:c(Cl):c:c:c:c:1NS(=O)(=O)c2:c:c:c3N[C@H]([C@@H]4CC=C[C@@H]4c:3:c:2)c5:c:c:c(:c:c:5)C(=O)O	2975144	48.532	4.3140	-9.3
18	OC(=O)c1:c:c:c(COc2:c:c:c(\C=C(\C#N)/c3:c:c:c:c(F):c:3):c:c:2Br):c:c:1	2229326	15.654	4.8054	-8
19	CCN1N=C(\C=C/c2:c:c:c:c:c:2)N=C3C(=O)N(C)C(=O)N=C13	5756371	11.704	4.9317	-7.5
20	CCCC1=NN(C)C2=NC(=O)N(C)C(=O)C2=N1	3164059	1.598	5.7964	-7.2
21	COc1:c:c:c(Cl):c:c:1C(=O)Nc2:c:c:c:c(:c:2)c3:c:c:c4:n:n:c:n:4:n:3	7217786	38.456	4.4150	-8.4
22	OC(=O)COc1:c:c:c(\C=N/NC(=O)c2:c:c:c(:c:c:2)c3:c:s:c(Nc4:c:c:c(Cl):c:c:4):n:3):c:c:1	9595032	1.24	5.9066	-7.9
23	N\C(=N\N=C/c1:c:c:c2OCOc:2:c:1)\S[C@H]3CC(=O)N(C3=O)c4:c:c:c(:c:c:4)C(=O)O	25250764	8.58	5.0665	-8.5
24	OC(=O)c1:c:c:c:c(:c:1)n2:c:c:c:c:2\C=C/3\NC(=O)N(C3=O)c4:c:c:c(Cl):c:c:4	6104167	4.404	5.3562	-7.9
25	COc1:c:c:c(\C=C/2\SC(=S)N(CCC(=O)Nc3:c:c:c(:c:c:3)C(=O)O)C2=O):c:c:1OC	1587127	2.755	5.5599	-7.9
26	OC(=O)c1:c:c:c:c(NC(=O)\C(=C/c2:c:c:c(OCc3:c:c:c(Cl):c:c:3):c:c:2)\C#N):c:1	1516220	6.424	5.1922	-7.9
27	Cc1:c:c:c(\C=C/C2=Nc3:s:c(C(=O)O):c(C):c:3C(=O)N2):c:c:1[N+](=O)[O-]	8853383	11.188	4.9512	-7.6
28	CCOc1:c:c(\C=C(\C#N)/C(=O)Nc2:c:c:c:c(:c:2)C(=O)O):c:c:c:1OCc3:c:c:c(Br):c:c:3	2354598	1.24	5.9066	-7.7

29	Cc1:c:c:c(:c:c:1NC(=O)c2:c:c:c3C(=O)N(C(=O)c:3:c:2)c4:c:c:c(:c:c:4)[N+](=O)[O-])C(=O)O	2867365	14.971	4.8247	-8.7
30	COc1:c:c:c(NC(=O)CN2C(=O)\C(=C\3/SC(=S)N(CCC(=O)O)C3=O)\c4:c:c:c:c:c2:4):c:c:1	1889464	13.791	4.8604	-7.6

Molecular alignment

In the building of the CoMFA (FFDSEL and UVEPLS) model, the arrangement of the chemical structure is of crucial importance [Edache et al., 2020]. The exactness of the CoMFA model estimates and the stability of the polyhedron map is highly dependent on the structural arrangement of the molecules [18, Edache et al., 20]. The structure of the most active stable compound was used as an archetype for superimposition, assuming that it is the most biologically active conformation at the active receptor site. In Open3DALIGN [19], the fragment was chosen from the Atom-based fashion and pharmacophore-based fashion alignment method and the majority of the molecules had been matched with it. Because of its high O3A score (see Table 2), compound 17 was chosen as the template to align other compounds in Figure 1.

Table 2. Open3DALIGN O3A_Score for each compound

Template	ID	Conformer	O3A_SCORE	Template	ID	Conformer	O3A_SCORE
1	1	1	3273.04	16	16	1	3342.30
2	2	1	2393.27	17	17	1	3343.85
3	3	1	2382.93	18	18	1	3057.57
4	4	1	3098.14	19	19	1	3298.92
5	5	1	2967.11	20	20	1	3141.24
6	6	1	3100.33	21	21	1	2813.51

7	7	1	2471.96	22	22	1	2786.13
8	8	1	2885.83	23	23	1	3073.36
9	9	1	2982.02	24	24	1	2983.43
10	10	1	3068.17	25	25	1	3149.42
11	11	1	2618.28	26	26	1	3101.67
12	12	1	3064.03	27	27	1	2915.27
13	13	1	2888.78	28	28	1	3111.94
14	14	1	2977.79	29	29	1	3169.11
15	15	1	3110.59	30	30	1	3103.32

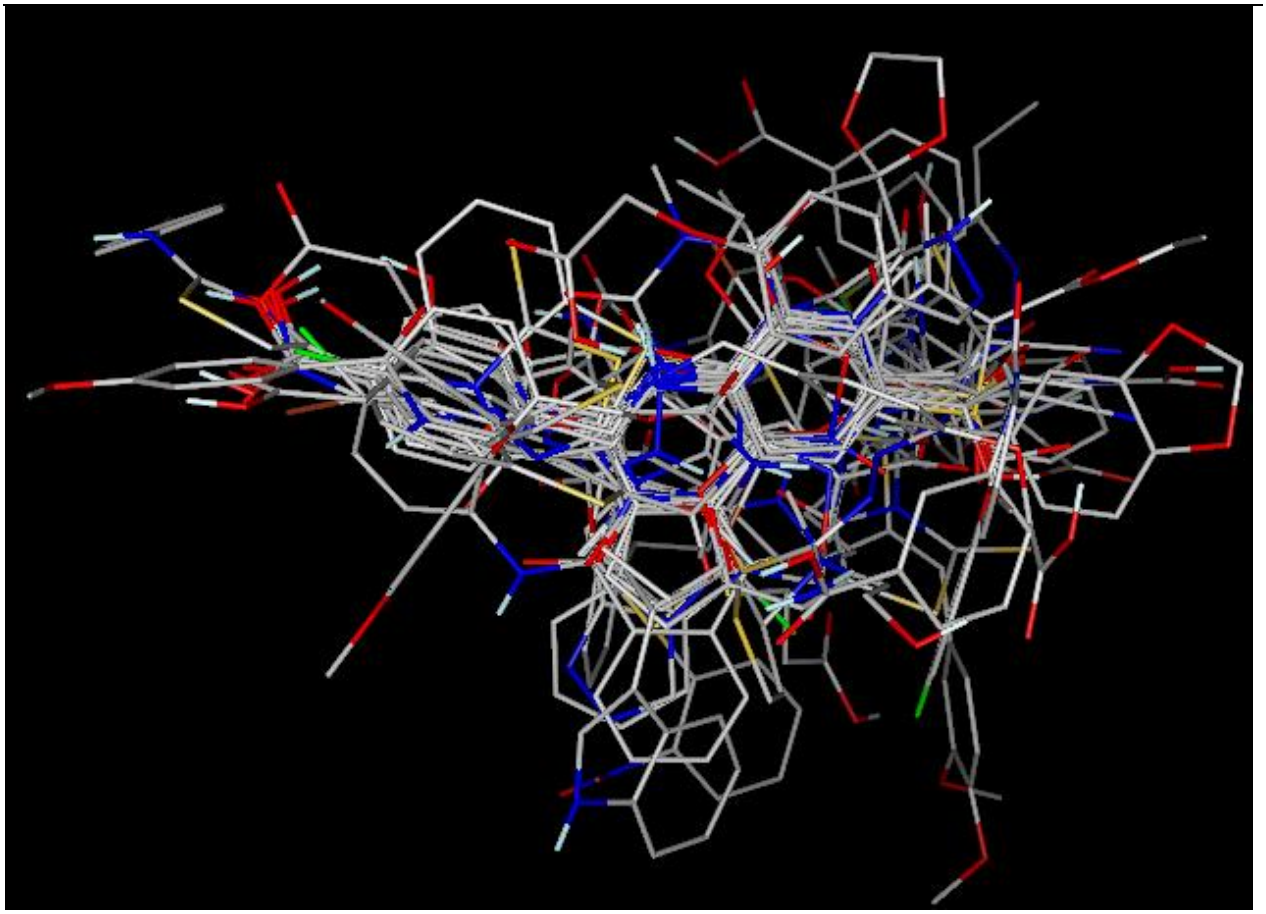

Figure 1. Superposition of 30 molecules in the training collection, including substances, and test collection on the prototype compound 17.

The 3D descriptors were used as independent variables and the pIC50 (biochemical activity) as the dependent variable to derive 3D-QSAR models. Open3DQSAR is used today for high-throughput MIFs analysis for pharmacophore exploration [20]. This Open3DQSAR approach can be used to evaluate pharmacophores and formulate drugs based on ligand [24]. Recent studies show that the research findings using this approach are similar to CoMFA and CoMSIA [18]. For Open3DQSAR research, Molecular Interaction Fields (MIFs) for steric and Coulomb interactions were calculated using a grid box with a phase size of 2Å and a distance of 5Å [18], similar to the CoMFA report. These MIF descriptors were pre-treat maximum and minimum cut-offs (level = ±30), zeroing (level = 0.05), standard deviation cut-off (level = 2.0), N-level variable exclusion, and block unscaled weighting (BUW). Finally, to compare the MIFs with the pIC50 operation, the fractional factorial design-PLS (FFDSEL) approach was employed. Using the uninformative variable elimination-partial least square (UVE-PLS) variable selection technique, the least informative variables were excluded from the model.

Preparation of target proteins

The 3D Structure of A “hotspot” for autoimmune T cells in type 1 diabetes (PDB code: 5HYJ) crystal structure [21] used in this study was extracted from the Protein Data Bank (PDB) of the RCSB (Research Collaboratory for Structural Bioinformatics). Using the Discovery Studio 2017 R2 Client, the heteroatom was removed from the 5HYJ protein PDB files. The 5HYJ polypeptide chains (B to J) were deleted and only the Homo sapiens chain A was saved for further study as a PDB file format. T cell antigen receptor (TCR) 5HYJ chain A has been used successfully to monitor and discover unique molecules for the treatment of type 1 diabetes [21]. The resolution of this entry mentioned is 1.85 Å.

Molecular docking Simulations Setup

We used the PyRx-Visual Screening Tool v0.8 docking program from the Scripps Research Institute. The Autodock Vina [26] was used to obtain the T cell [21] receptor protein's affinity energy and binding mode with the compounds (Table 1). The Drug Screening module is set with the Default parameters such as Exhaustiveness = 8, vina search space (center_x = 24.8398, center_y = -49.82, center_z = 103.4175), dimensions in angstrom (size_x = 47.1821511173, size_y = 55.8864878082, and size_z = 70.2009980774). For further investigation, the ligand validation with the least binding energy was chosen. The discovery studio client R7 program was used to image and analyze protein-ligand complexes.

Molecular Dynamic Simulations Setup

Molecular dynamics simulations are performed using VMD [22] and NAMD [23] and the CHARMM force field [24]. The CHARMM27 force field was used to calculate the interaction parameters. To measure the solvated protein, the periodic boundary condition was used and the device was immersed in a cubic water box of extended simple point charge water molecules. The protein was solvated with explicit water with 0.15M NaCl salt concentration for neutralization. To maximize the initial structure of the protein, minimization was performed. After that, the system temperature was steadily heated up by 100ps from 0 K to 310 K. Finally, at 310 K for 100ps with the NVT ensemble, the system was balanced. The system was simulated for 1ns (500,000 steps) of chemical time. The MD simulation and results from the analysis were performed on the DELL INSPIRON; Pentium® Dual-Core CPU T4500 @ 2.30GHz and 3GB of RAM, 64-bit-Operating System, x64-based processor. A full summary of the input parameters is given in the NAMD documentation (www.ks.uiuc.edu/Research/namd/).

Results and Discussion

Best subset selection-multiple linear (BSS-MLR) regression techniques were used to pick the most important descriptors. Two models with a training set of 21 compounds (70%) and a test set of 9 compounds (30%), were selected from the numerous built model, with three (3) descriptors, the next to the ratio of the five training molecules for each descriptor with low generality and prediction ability for the test set. With the selected descriptors, using the training data set, we developed the linear 2D-QSAR model and obtained the following equations (models 1 and 2), as shown below. Models 1 and 2 present this equation as well as its statistical parameters. The prediction results were obtained using the test set.

Model 1

pIC_{50} = 2.91569(+/-0.74036) - 0.66691(+/-0.21349) **ATSC1e** -0.01851(+/-0.00887) **AATSC6m** +6.85628(+/-2.56507) **BCUTc-1h** _____**Model 1**

Parameters for Internal Validation: SEE = 0.3431; r^2 = 0.7072; r^2 adjusted = 0.6556; F = 13.68798 (DF: 3, 17)
Leave-One-Out (LOO) Result: Q2 = 0.6113; PRESS = 2.6563; SDEP = 0.3557

Parameters for External Validation: RMSEP = 0.3160; Rpred^2 = 0.6157; Q2f1 = 0.6157; Q2f2 = 0.5062

Appropriate model requirements for Golbraikh and Tropsha:
K = 1.0066; [(r^2-r0^2)/r^2] = 0.02222 OR* K' = 0.99001; [(r^2-r'0^2)/r^2] = 1.53668 Passed

Model 2

pIC_{50} = 3.3212(+/-0.46284) - 0.02397(+/-0.008) **AATSC6m** +3.11153(+/-0.66862) **GATS1e** -0.10704(+/-0.02624) **nTRing** _____**Model 2**

Parameters for Internal Validation: SEE = 0.3227; r^2 = 0.7409; r^2 adjusted = 0.6952; F = 16.20625 (DF: 3, 17)
Leave-One-Out (LOO) Result: Q2 = 0.6481; PRESS = 2.4048; SDEP = 0.3384

Parameters for External Validation: RMSEP = 0.3192; Rpred^2 = 0.6079; Q2f1 = 0.6079; Q2f2 = 0.4962

Appropriate model requirements for Golbraikh and Tropsha:
K = 1.0123; [(r^2-r0^2)/r^2] = 0.0034 OR* K' = 0.9845; [(r^2-r'0^2)/r^2] = 1.09102 Passed

Where the cut-off point: [0.85 < K < 1.15 and ((r^2-r0^2)/r^2) < 0.1] OR* [0.85 < K'< 1.15 and ((r^2-r'0^2)/r^2) < 0.1], respectively.

Table 3 shows the experimental and expected values based on the BSS-MLR model. Figure 2 also displays the expected versus experimental pIC_{50} for all 30 compounds in the training and test sets. Table 3 shows that the predicted and experimental values for the pIC_{50} are in good agreement. Model 1 had an explanatory power of about 71 percent and a standard error of estimation (SEE) of 0.34, R2adjusted = 0.66, and Fischer ratio (F) =13.69, while model 2 had an explanatory power of 74 percent and a least standard error of estimation (SEE) of 0.32, R2adjusted = 0.70, and Fischer ratio of 16.21. To assess the predictive potential of the BSS-MLR model, the correlation coefficients of cross-validation (Q2) and external validation (R2pred) were calculated. Internal validation Q2 = 0.61, SDEP = 0.36, R2pred = 0.62, RMSEP = 0.32 in model 1, and Q2 = 0.65, SDEP = 0.33, R2pred = 0.61, RMSEP = 0.32 in model 2. Because of its low standard error of estimate (SEE) and strong leave one out cross-validation (Q2(LOO)), model 2 appears to be more promising.

Table 3. Descriptors and predicted activity of training and test set (Model 1 & 2)

Name	ATSC1e	AATSC6m	BCUTc-1h	GATS1e	nTRing	pIC50	Predicted pIC50 (1)	Predicted pIC50 (2)
2	-0.45138	3.05046	0.27678	0.88411	6	5.078	5.0537	5.4579
3	0.74477	-2.84469	0.22321	0.44417	3	4.208	3.8900	4.5508
4	-0.08241	-3.21612	0.2969	0.75940	14	4.20798	5.1115	4.3485
5	-0.2239	-32.2562	0.33074	0.72502	3	5.90658	5.952356	6.152657
6	-0.1358	-12.4722	0.33041	0.69289	3	5.90658	5.446754	5.407724
7	0.19233	0.417906	0.34799	0.63054	0	5.38977	5.049686	5.239743
8	-0.38076	-14.9168	0.25911	0.78250	5	5.32121	5.178894	5.622514
9	0.41466	1.61963	0.2765	0.52287	7	4.237659	4.547774	4.138233

10	0.25223	-7.20262	0.30337	0.58702	5	5.025626	4.953348	4.760256
11	0.37966	5.463707	0.25721	0.61454	4	4.882464	4.212506	4.642147
12	-0.67338	-3.17678	0.32654	0.8221	3	5.620876	5.671898	5.636821
13	0.30992	0.494154	0.25062	0.63265	3	4.425078	4.41704	5.012047
16	-0.73162	-6.12185	0.30048	0.79517	7	5.694649	5.546223	5.118679
17	0.09184	1.393156	0.29075	0.59667	8	4.313972	4.866433	4.282581
19	0.06084	-10.2925	0.33044	0.63369	4	4.931666	5.39702	5.126383
20	-0.00932	-16.8192	0.33042	0.65751	3	5.796423	5.435354	5.390307
21	0.08544	-1.33157	0.23805	0.68989	5	4.415036	4.538309	4.997014
24	-0.48518	0.621487	0.29193	0.73625	4	5.356153	5.208899	5.151033
25	-0.53385	9.345455	0.32654	0.80649	3	5.559878	5.231667	5.172499
26	-0.35188	-8.67198	0.2908	0.74360	3	5.192194	5.316509	5.554288
29	0.23877	-6.02456	0.29085	0.56797	5	4.824749	4.865343	4.682246
				Test set				
1	0.01855	-14.3822	0.33043	0.64053	4	4.98209	5.435002	5.230721
14	-0.29547	-5.9311	0.33644	0.81101	4	5.32948	5.529199	5.558663
15	-0.38816	0.552731	0.33641	0.81476	6	5.90658	5.470832	5.200831
18	-0.23976	7.281604	0.29072	0.67549	3	4.80538	4.934079	4.92738
22	-0.36514	-9.48536	0.33639	0.77472	4	5.90658	5.641126	5.530903
23	-0.63997	4.112573	0.29076	0.81903	5	5.06651	5.25989	5.235873
27	0.27425	-2.0606	0.29781	0.57235	4	4.95125	4.812766	4.723306
28	-0.38016	-10.3838	0.29082	0.79061	3	5.90658	5.3553	5.708938
30	-0.57066	5.116052	0.26049	0.76043	5	4.86040	4.987564	5.029467

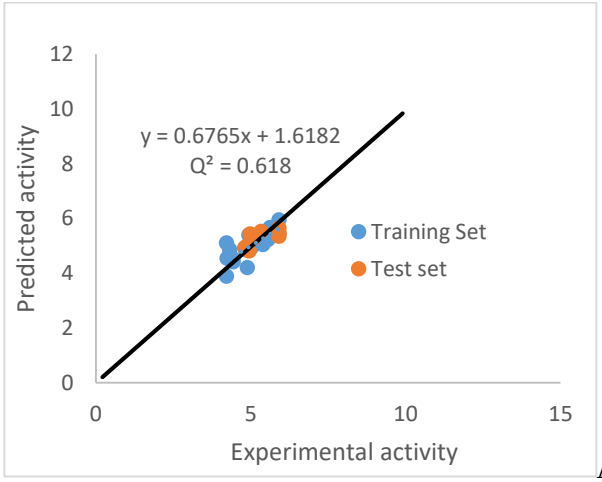

A

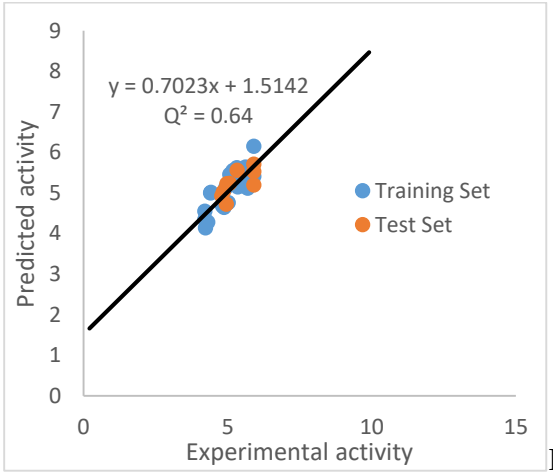

B

Figure 2. Actual and predicted activities for training and test set molecules are plotted on a graph (A) Model 1 (B) Model 2

The Y-randomization test was carried out to avoid the chance correlation and to ensure that the models are robust [25]. After several reshuffles of the obtained 2D-QSAR model (Table 4 and 5), the R, R2, and Q2 values differ [26]. The deviation in the values of the non- disarrange model's squared mean correlation coefficient (R2) from the disarranged model's squared correlation coefficient (cRp2) is expressed in the value of cRp2 = 0.65 for the model 1 and 0.66 for model 2. Both are more bang-up than 0.5, indicating that the original 2D-QSAR models have a high level of internal consistency. External statistically validation parameters like Q2f1, Q2f2, K, [(r2-r02)/r2], K', and [(r2-r'02)/r2] that beat the threshold values defined by Golbraikh and Tropsha [27] indicate acceptable predictability of the held 2D-QSAR models.

Table 4. R^2 train, Q^2_{LOO}, and cRp^2 values after several Y-randomization tests for model 1.

Model 1	R	R^2	Q^2
Original	0.8410	0.7072	0.6113
Random 1	0.5349	0.28616	-0.1375
Random 2	0.2144	0.0460	-0.6585
Random 3	0.1231	0.0152	-0.5837
Random 4	0.2659	0.0707	-0.3859
Random 5	0.1994	0.0398	-0.4672
Random 6	0.4009	0.1607	-0.3855
Random 7	0.1559	0.0243	-0.6550
Random 8	0.1440	0.0208	-0.6674
Random 9	0.5850	0.3423	0.0658
Random 10	0.5570	0.3103	-0.0535
Random Models Parameters			
Average r :		0.3181	
Average r^2 :		0.1316	
Average Q^2 :		-0.3928	
cRp^2 :		0.6547	

Table 5. R^2 train, Q^2_{LOO}, and cRp^2 values after several Y-randomization tests for model 2.

Model 2	R	R^2	Q^2
Original	0.8608	0.7409	0.6481
Random 1	0.3089	0.0954	-0.4211
Random 2	0.3846	0.1479	-0.2874
Random 3	0.5320	0.2830	-0.0350
Random 4	0.1922	0.0369	-0.5226

Random 5	0.6204	0.3849	0.0177
Random 6	0.5221	0.2726	-0.0244
Random 7	0.2920	0.0852	-0.4960
Random 8	0.3443	0.1185	-0.3042
Random 9	0.6377	0.4066	0.1021
Random 10	0.1540	0.0237	-0.7533
Random Models Parameters			
Average r :	0.3988		
Average r^2 :	0.1855		
Average Q^2 :	-0.2724		
cRp^2 :	0.6566		

The multi-collinearity between the above descriptors (model 1 and 2) was identified by measuring their variance inflation factors (VIF). If VIF equals 1, there is no inter-correlation for each variable; if VIF falls between 1 and 5, the related model is acceptable; and if VIF exceeds 10, the related model is unstable and a recheck is needed [28]. Tables 6 and 7 display the corresponding VIF values for each of the three descriptors for models 1 and 2. Tables 6 and 7 show that all of the descriptors have VIF values of less than two (2), suggesting that the model is statistically significant and that the descriptors are sufficiently orthogonal. The mean effect (MF) for models 1 and 2 is shown in Tables 6 and 7, respectively. The MF indicates the relative importance of a descriptor and its percentage contribution were compared with each other descriptors in the models. Its sign denotes the variable direction in the values of activities as a result of the calculated descriptor values increasing or decreasing. Model 1 shows that decreasing the value of Centered Broto-Moreau autocorrelation - lag 1 / weighted by Sanderson electro-negativities (ATSC1e) by 2%, and Average centered Broto-Moreau autocorrelation - lag 6 / weighted by mass (AATSC6m) by 4% increase the biological activity. The MF of nlow highest partial charge weighted BCUTS (BCUTc-1h) shows that biological activity increases by increasing 94% of the descriptor. In model 2 Table 4, a decrease of these descriptors, Average centered Broto-Moreau autocorrelation - lag 6

/ weighted by mass (AATSC6m) by 4% and Number of rings (includes counts from fused rings) (nTRing) by 18% increases the bioactivity of the compounds. An increase in Geary autocorrelation - lag 1 / weighted by Sanderson electronegativities (GATS1e) by 78% increase the biochemical activity of the compounds.

Table 5: Linear model 1 is based on the three parameters selected by the BSS-MLR method.

Descriptor	VIF	Mean effect	Contribution (%)
ATSC1e	1.209	-0.0191	~ 2
AATSC6m	1.114	-0.0423	4
BCUTc-1h	1.327	0.9386	94

Table 6: Linear model 2 is based on the four parameters selected by the BSS-MLR method.

Descriptor	VIF	Mean effect	Contribution (%)
AATSC6m	1.024	-0.067	4
GATS1e	1.019	1.22	~ 78
nTRing	1.036	-0.287	18

The leverage values for each compound can be calculated and plotted against uniform residues, allowing for graphical recognition of both outliers and prominent compounds in the model. The applicability domain (Williams plot) is based in a squared/rectangular region in the 2 or 3 bound for residuals and the threshold value h*, which can be mathematically represented as $h^* = (3p+1)/c$, where p is the number of model parameters and c is the number of compounds [29, 30]. All of the compounds from the training and test sets are contained within this square / rectangular area, as shown in Model 1 Figure 3a. There are no outlier and influential compounds with standardized residues -3 and +2 for both training and test sets. In comparison, both substances have a value

smaller than the alert value h* of 0.50. In model 2 Fig. 3b, all the compounds fall within the leverage threshold value (of 0.5) except compound 4 (training set). From the figure, they are no influential compounds with a standardized residual of ±3.

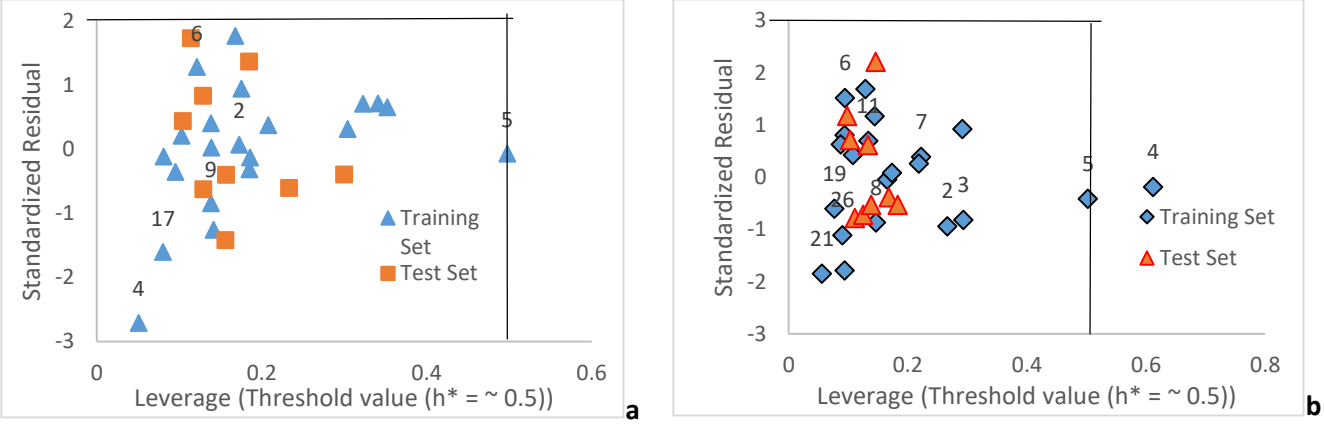

Figure 3. The Williams map, which shows the uniform residuals against the leverage value (a) model 1 (b) model 2.

Results of the 3D-QSAR models

The steric (van der Waals) and electrostatic (coulombs) descriptors were used to create the 3D-QSAR models, which provide easy understanding and chemical transferability. Table 8 displays the best CoMFA fractional factorial architecture (ffdsel) and CoMFA uninformative variable elimination-PLS (uvepls). For the CoMFA (ffdsel) model, the partial least square (PLS) analysis revealed a high leave one out (Q2) value of 0.5645 with 5 components. The convectional R2 of 0.9982, F-value of 1659.5690, and leave two out (Q2LTO) of 0.5372 with leave many out cross-validation (Q2LMO) of 0.4783 was obtained from the non-cross-validated PLS analysis. The working MIFs model was chosen as the CoMFA (uvepls) model, which uses both steric and electrostatic fields on 2.0 grid spacing, and whose validity and predictability were assessed by the R2 value of 0.9989 and Q2 value of 0.6307 with 5 components, F-value of 2679.6896, Q2LTO value of 0.6077, and leave many out cross-validations (Q2LMO) of 0.5466 (Table 7), which

indicated that the obtained 3D-QSAR model is reliable and able to predict binding affinities of the new compound.

Table 8: Summary of 3D-QSAR models parameters

Statistical parameters	CoMFA (ffdsel)	CoMFA (uvepls)
R^2 (SDEC)	0.9982 (0.024)	0.9989 (0.0189)
Q^2_{LOO} (SDEP)	0.5645 (0.3722)	0.6307 (0.3428)
Q^2_{LTO} (SDEP)	0.5372 (0.3837)	0.6077 (0.3533)
Q^2_{LMO} (SDEP ± SD)	0.4783 (0.4066 ± 0.0266)	0.5466 (0.3789 ± 0.0268)
F-test	1659.5690	2679.6896

Interpretation of 3D-QSAR contour map

Both steric and electrostatic fields made different contributions in these CoMFA models. The van der Waals (steric) and Coulomb (electrostatic) contributions were found to be 77.7% and 22.3 percent, respectively, in CoMFA (ffdsel). The van der Waals and Coulomb contributions were found to be 55.03 percent and 44.97 percent, respectively, in CoMFA (uvepls). As a result, the steric field had a greater impact than the electrostatic field, implying that steric interactions between molecules and receptors could be a key factor in anti-diabetes activity. Figures 4a and 4b display the plots of experimental and expected behavior obtained from CoMFA (ffdsel) and CoMFA (uvepls) studies, respectively.

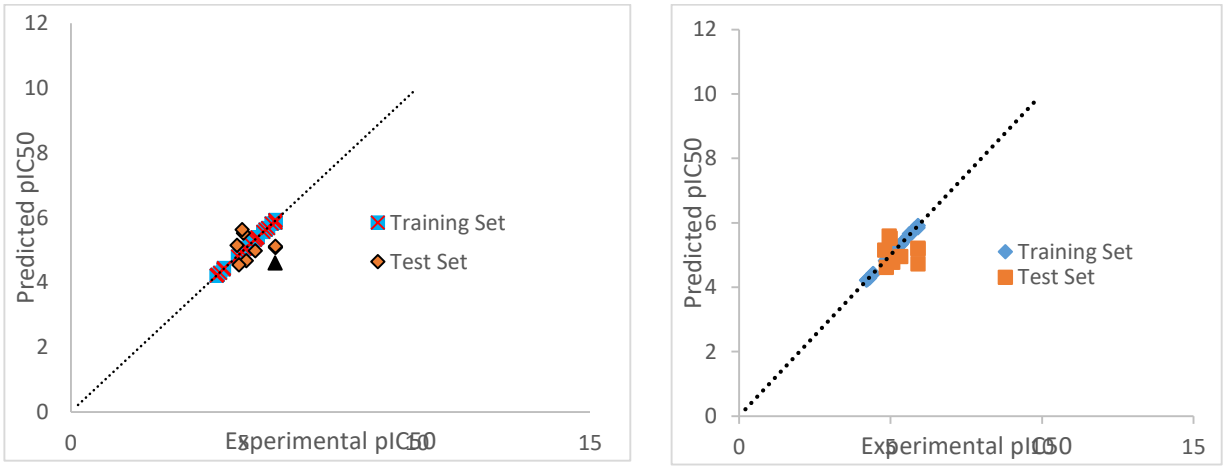

Figure 4. Scatter plots of pIC50 3D-QSAR models for the training sets and test set validation

Furthermore, 3D-QSAR models offer a way to explain the wealth of information derived from MIFs generated by 3D-QSAR models. Figures 5, 6, 7, and 8 depict the contour maps produced during pharmacophore evaluation and drug formulation-based Open3DQSAR analyses. The contour maps represent the favored and disfavored region in the molecular space that influences the biochemical activity of the molecules. The steric and electrostatic contours of CoMFA (ffdsel) compounds with the lowest activity (compound 5) and the highest activity (compound 17) are shown in Figures 5 to 8. The green and red polyhedrons signify regions in molecular space in which increased or decreased steric groups, respectively, are estimated to improved bioactivity in CoMFA (ffdsel) steric interactions contour maps of lowest biochemical activity (compound 5) and highest biochemical activity (compound 17). In the steric contour map of compound 5, a large green polyhedron suggesting increased steric bulk was located away from the structure, whereas because of the molecular size and functional groups attached, this steric bulk was found making interaction with the structure in the ffdsel steric contour map of compound 17. (Figure 5 and 6). The blue and yellow polyhedrons in the electrostatic counter map (Figures 5 and 6) indicate regions of higher electron density with a high binding affinity (negative charge) and lower electron density

with a lower affinity of the compounds to bind the protein (partial positive charge), respectively, predicting activity enhancement with compound 5 (low activity) and compound 17 (high activity), respectively.

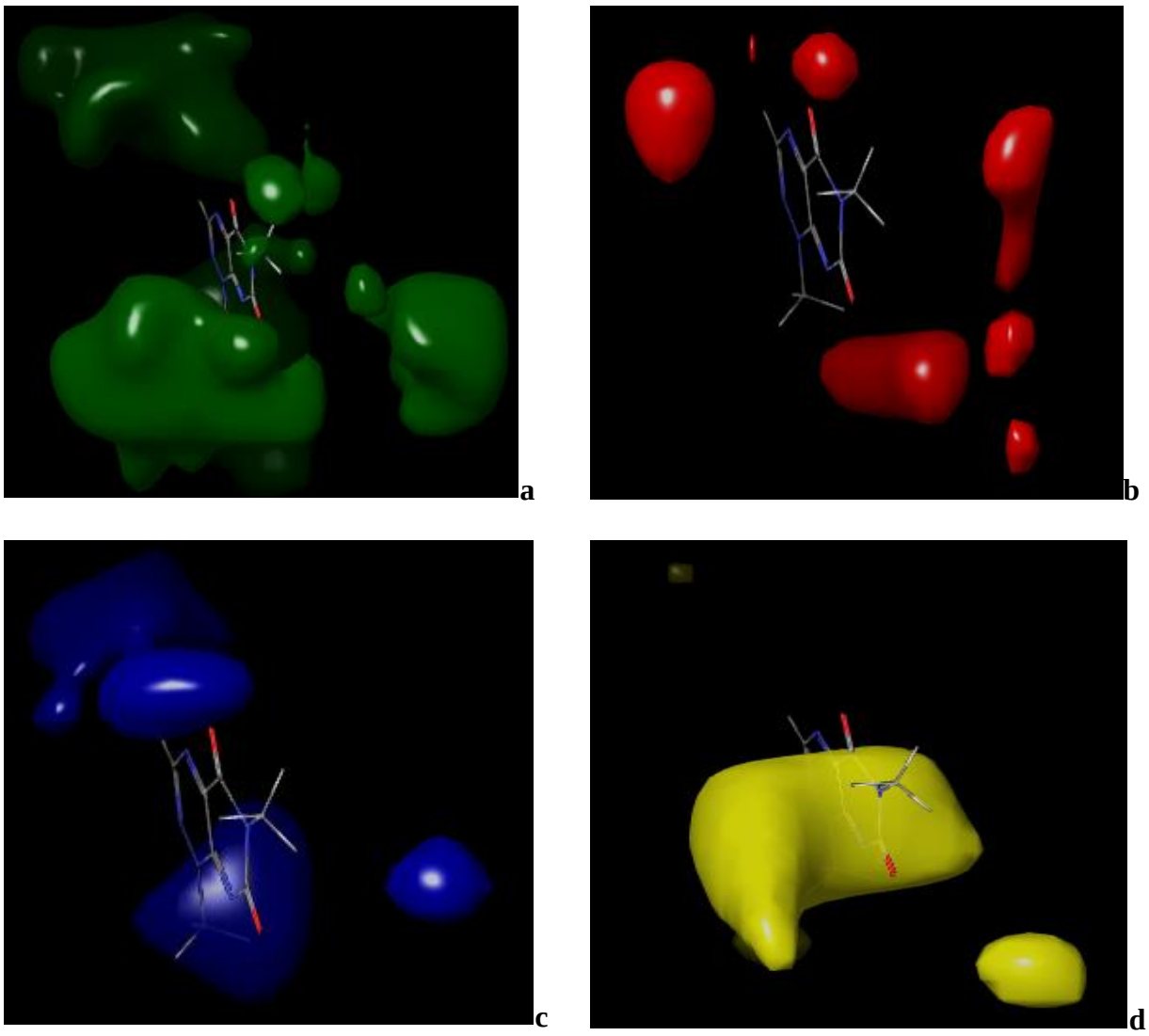

Figure 5. The CoMFA (ffdsel) steric (a) favorable (b) unfavorable and electrostatic interactions (c) electron-donating group (d) electron-withdrawing contour maps with the lowest binding affinity (compound 5).

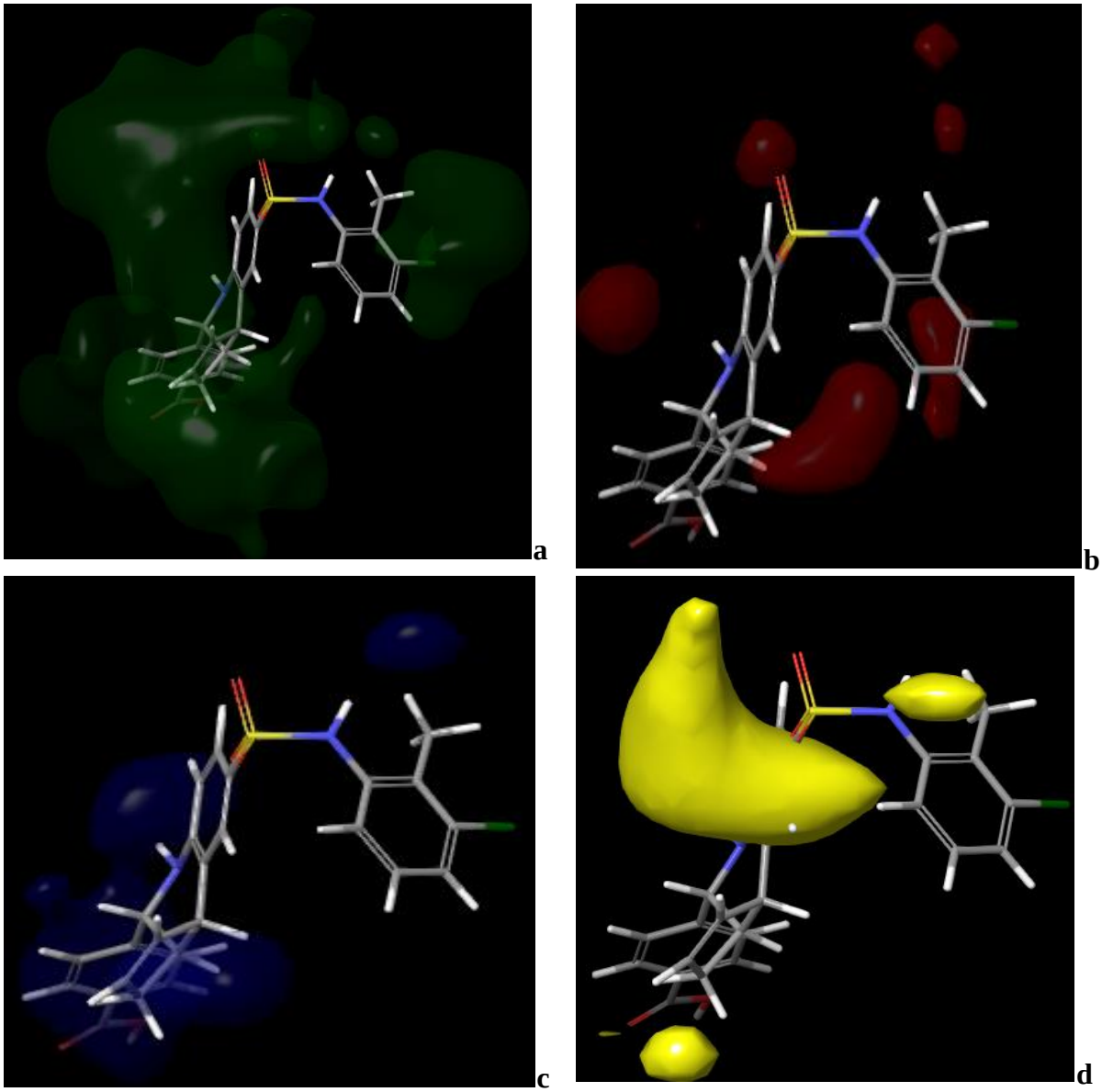

Figure 6. CoMFA (ffdsel) steric (a) favorable (b) unfavorable and electrostatic interactions (c) electron-donating group (d) electron-withdrawing contour maps with the lowest binding affinity (compound 17).

The CoMFA (uvepls) models for the two activities under review are relatively similar, suggesting that the putative biological receptor sites are related but vary enough to require considerable selectivity in some substances, as seen in the previous CoMFA (ffdsel) parts. In the CoMFA (uvepls) steric contour map of compound 5 (red contour), indicating increased steric bulk was located to the compound whereas in the CoMFA (uvepls) steric contour map of compound 17, this

steric bulk was found making interaction with the ligand. The closer the contour map to the ligand or molecule, the higher the steric energy. Both the favorable and unfavorable contour map of compound 5 (Figure 7a & 7b) are far apart from the compound, that is, they low steric (van der Waals) energy. The blue and yellow contour map of compound 5 (low activity) are the favorable electrostatic interactions with charged probe indicate molecular regions which are negative, and unfavorable electrostatic interactions with the positively charged probe indicate molecular regions which are positive, respectively.

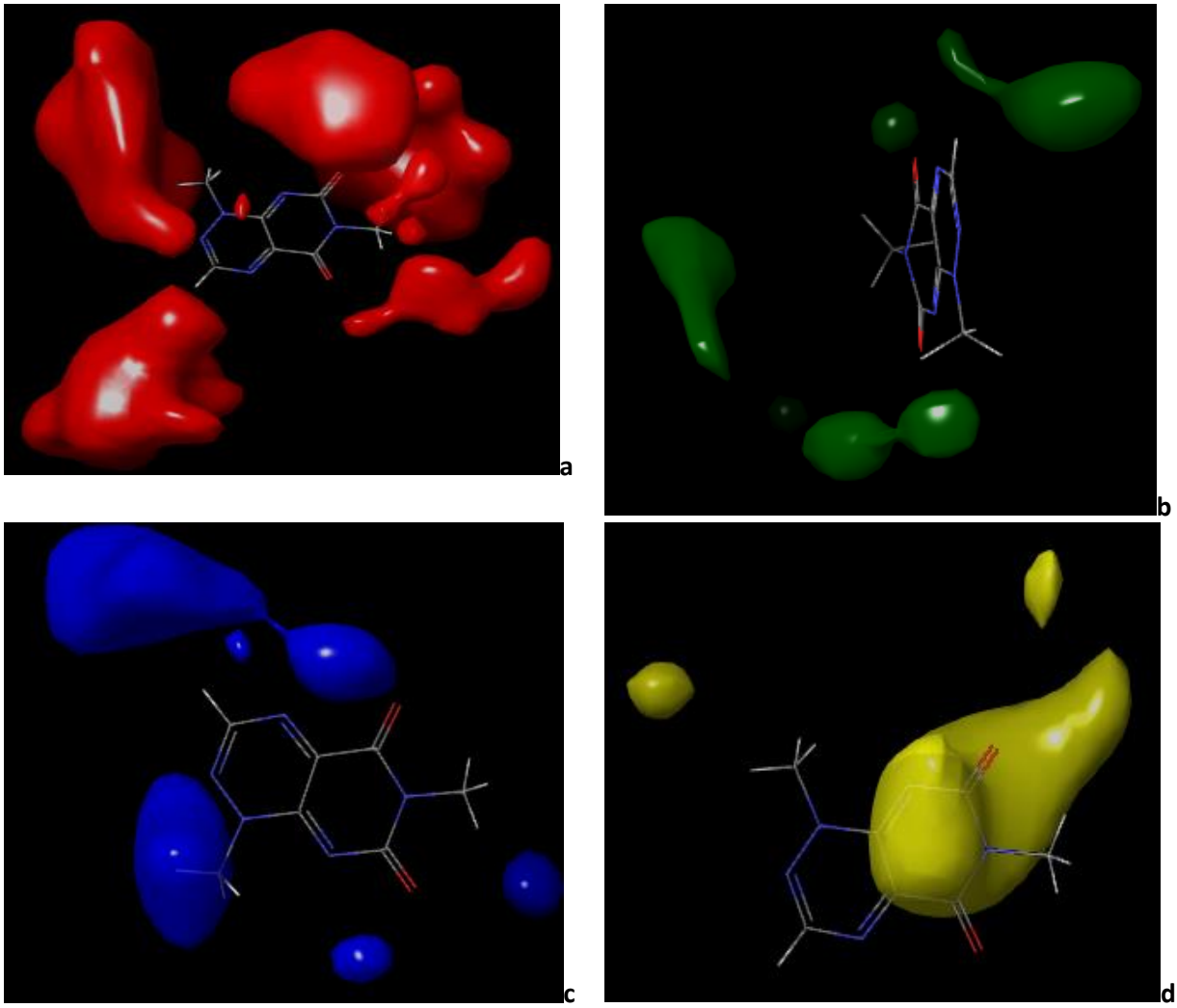

Figure 7. The CoMFA (uvepls) steric (a) favorable (b) unfavorable and electrostatic interactions (c) electron-donating group (d) electron-withdrawing contour maps with the lowest binding affinity (compound 5).

The contour maps of electrostatic interactions (Figure 7c and 7d) may explain why the activity of these compounds is different from compound 17 (Figure 8c and 8d). The contour maps are so close to compound 17 than compound 5. These show that the contour map is favorable for the interaction with the higher electron density with a high binding affinity (negative charge) and lower electron density with less affinity of the compounds to bind the protein (partial positive charge), respectively. This may explain why compound 5 is less potent than compound 17, which has a larger molecular size and more functional groups. As a result, these CoMFA models show that adding functional groups to a compound increases its activity, making it more potent.

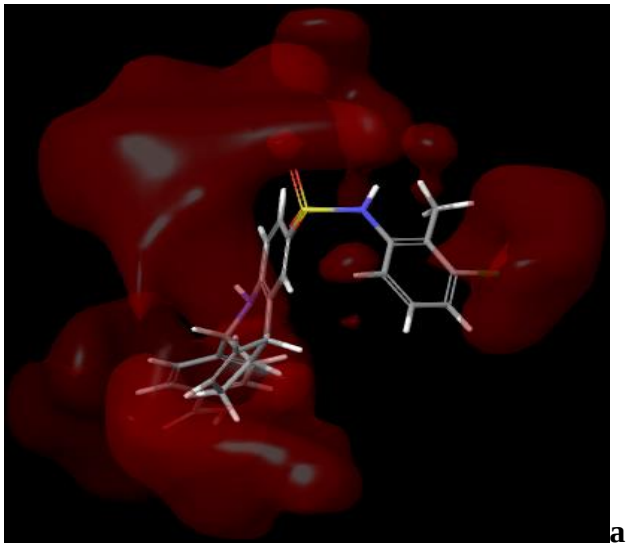

a

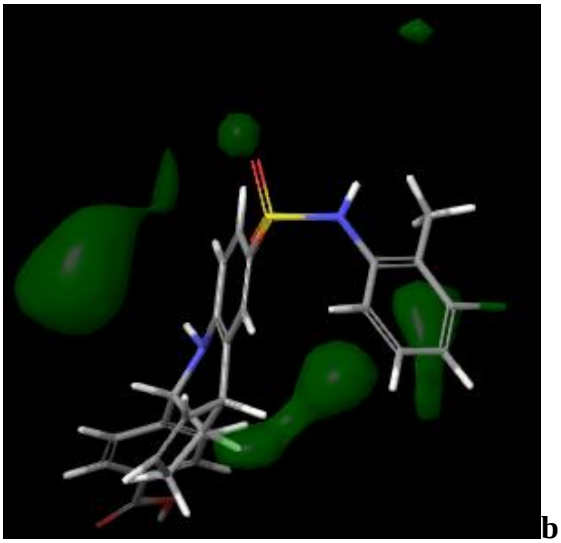

b

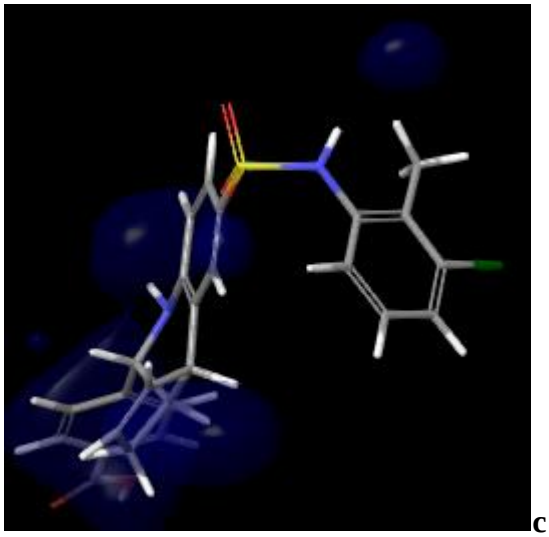
c
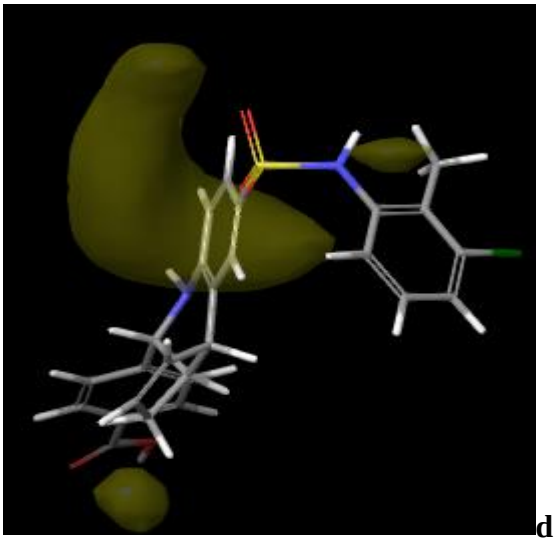
d

Figure 8. The CoMFA (uvepls) steric (a) favorable (b) unfavorable and electrostatic interactions (c) electron-donating group (d) electron-withdrawing contour maps with the lowest binding affinity (compound 17).

Interpretation of Molecular Docking Results

Molecular docking has become an essential tool in the drug designing process. The application of *in-silico* docking has received considerable attention because it has decreased the expense and time, by increasing the speed and efficiency of the drug discovery process [31]. The derivatives were docked to the autoimmune T cells in the type 1 diabetes enzyme (PDB code: 5HYJ) and the energy values were computed using PyRx (Autodock vina). The outcome of docking studies is presented in Table 1. The energy values obtained were ranged from -4.9 to -9.3 Kcal/mol. The results indicate that compound 17 (-9.3 Kcal/mol) exhibited promising inhibitory activity in comparison to other compounds. The compounds interact with the structure of the autoimmune T cells in type 1 diabetes by binding with van der Waals (Thr73, Ala69, and Trp167), electrostatic (Arg97 and Lys66), hydrophobic (Tyr159, Lys66, Tyr99, His114, Val152, and Trp147) i.e., Pi-sigma, Pi-Alkyl, and Alkyl, conventional hydrogen bonding (Arg97, Tyr159, and Glu63), carbon-hydrogen bond (His70) and miscellaneous interaction i.e., Pi-sulfur (His70) amino acid residues as shown in Figure 9a and 9b. These findings back up the findings of the CoMFA study, which

showed the significance of molecular size and functional groups (bulky group, electron donor, and electron acceptor) for a potentially active compound.

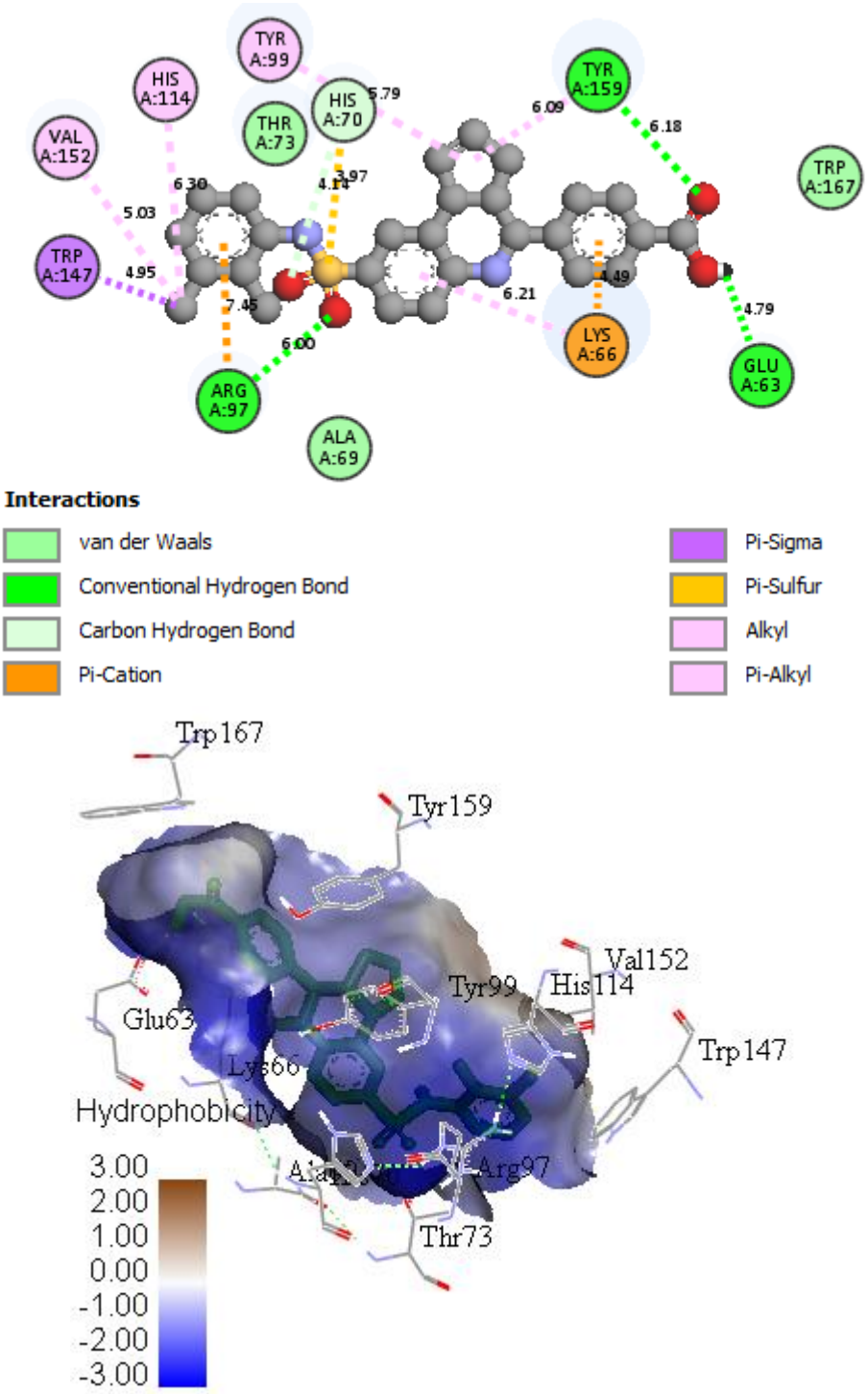

Figure 9. The docking interaction between compound 17 and the binding site of T cell in type 1 diabetes

Interpretation of MDs Simulation

By examining the results of 3D-QSAR and molecular docking, compound 17 was utilized as the lead compound, and the predominant changed area dictated by the above outcomes was almost altered with MD simulation. The root means square deviation (RMSD) and radial distribution function or pair correction function (RDF) plot of protein during the MD simulations are shown in Figure 10. The simulation result reveals that the RMSD tends to be steady and wavered at about 2.22 Å and relatively stable after 1ns (Figure 10A), the RDF is a system of the particle (protein) that describes how density varies as a function of distance from the reference particle (water). The RDF is usually determined by calculating the distance between all particle pairs and binning them into a histogram. The RDF was stable from a distance (r) of 0.05 to 1.25 (Å), then fluctuate at about 1.75 (Å) (Figure 10B). After running 500,000 steps (1ns) the RDF value was 0.594 at a distance (r) of 10.05 (Å), which implies that the structure of the complex is basically in a stable state as shown in Figure 10B.

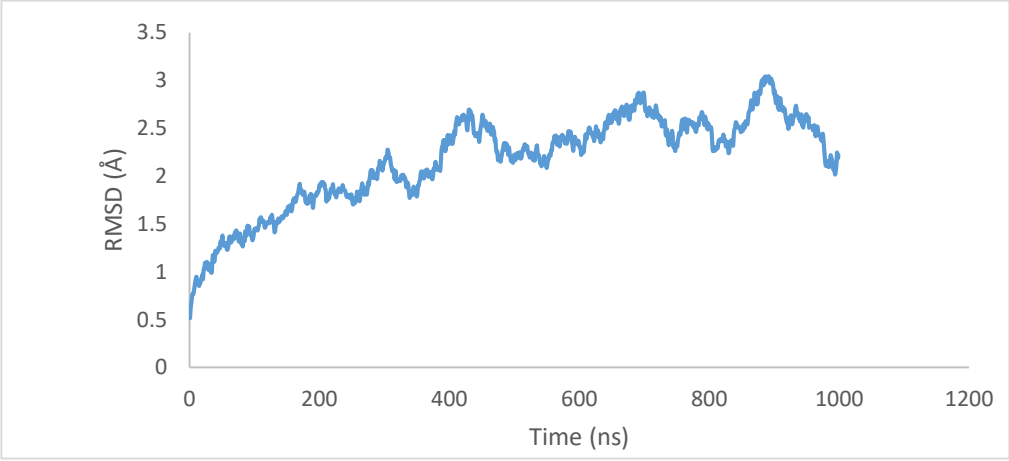

A

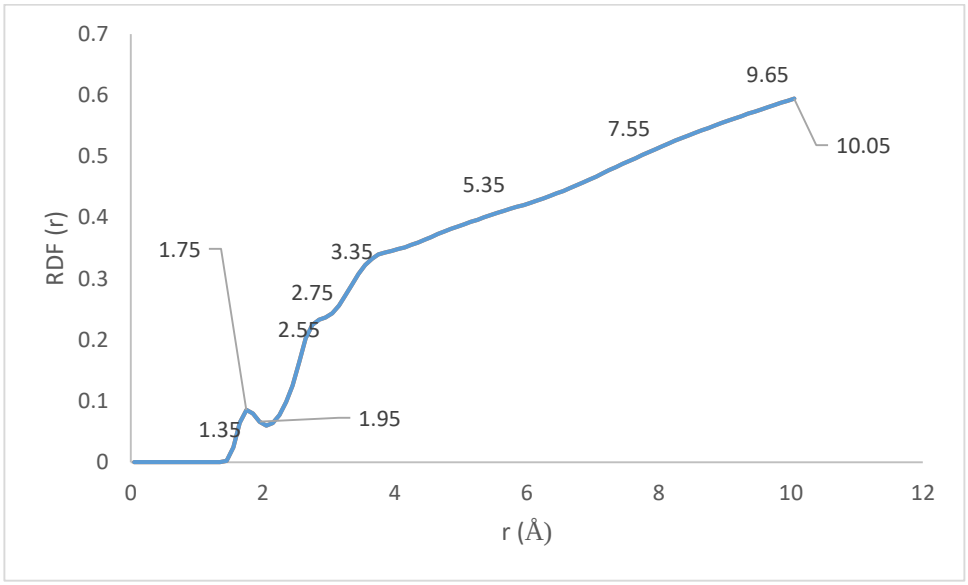

B

Figure 10. The product of molecular dynamic simulations during the 1ns NVT package. (A) The RMSD, (B) The Radial distribution function (RDF) value of the protein diagram.

Total energy, potential energy, temperature, and kinetic energy were monitored during the simulations to ensure the stability of the simulated system, and plots are shown in Figure 11A-11C.

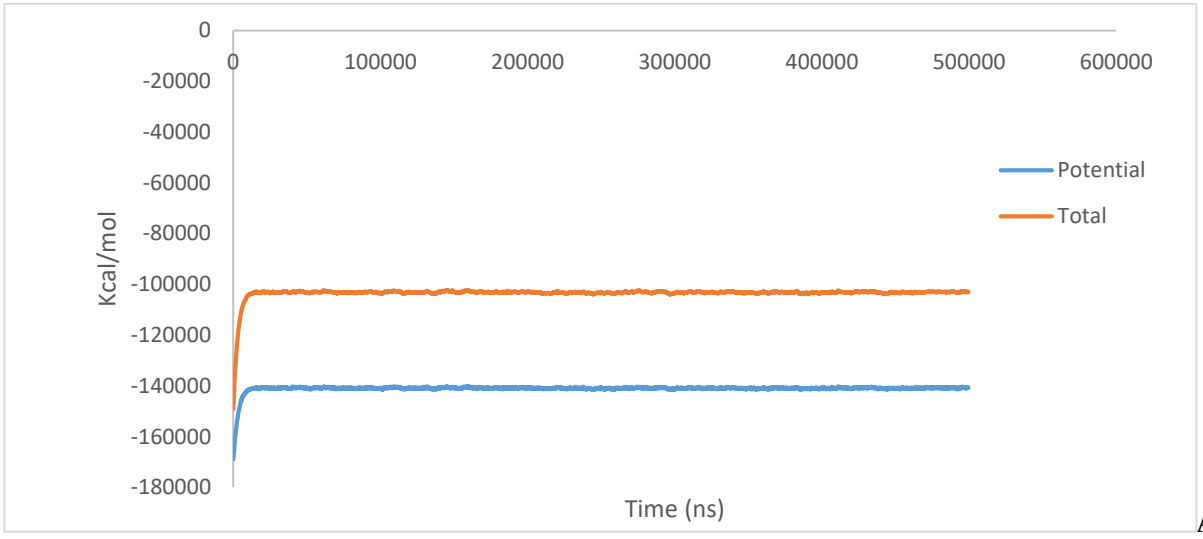

A

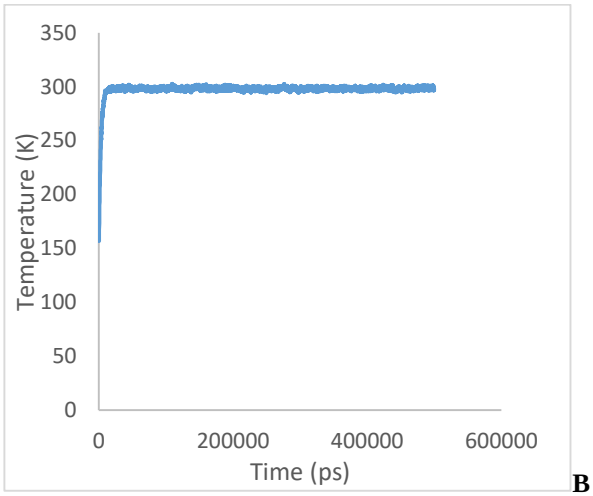

B

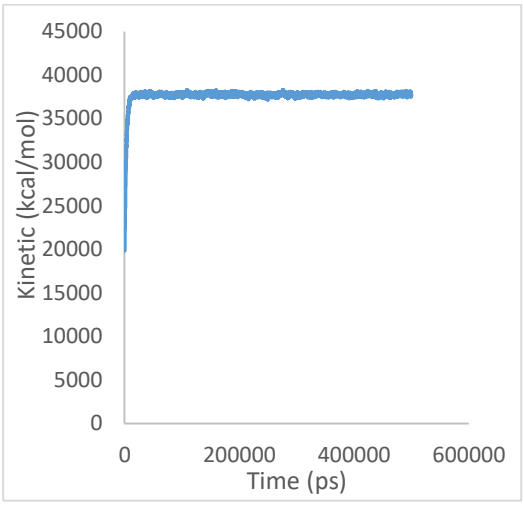

C

Figure 11. Plot of the simulated complex (A) Total /potential energy, (B) Temperature (C) kinetic energy

The Total energy, potential energy, and kinetic energy of the complex were set at -103070.17 KJ/mol, -140885.90 KJ/mol, and 37814.72, respectively. As shown in the same figure, the Total energy, potential energy, and kinetic energy of the system are stable and did not show any abnormal fluctuation during the entire MD simulation at a temperature of about 298.79K (Figure 11B). In conclusion, the complex was stable throughout the MD simulation. The protein-ligand interactions analysis is employed to explore more details about interactions between simulated protein and compound 17 during the 1ns MD simulation. In Figure 12, the ligand binding to protein in the same place with the docking model (Figure 9) and more deeply with the protein with additional interaction of pi-pi T-shaped and Amide-pi stacked. These additional interactions may increase this binding affinity. The MD simulation studies indicate that the bulky group, electron donor, and electron acceptor are very important for type 1 diabetes inhibition, the hydrogen-bonded interactions of the compound with amino acids of the target protein were also favorable.

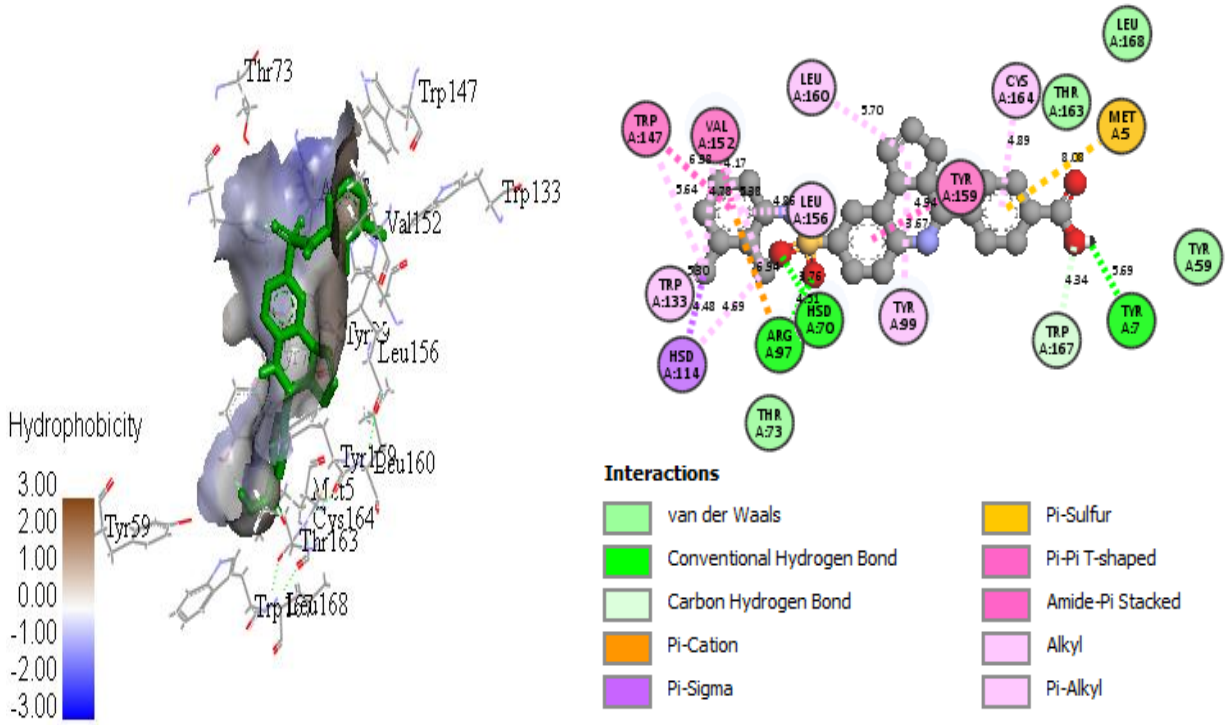

Figure 12. Molecular docking interactions of compound 17 with simulated protein structure.

Conclusions

In this research, the systematic investigation of 2D, 3D QSAR, docking simulation on thirty (30) compounds for autoimmune T cells in type 1 diabetes inhibitors is described. PaDEL-descriptor software packages were used to generate the 2D descriptors. The Data pre-treatment method and the Best subset selection (BSS) technique were used to filter the most appropriate descriptors. Multiple linear regression (MLR) was used to create two models (model 1 and model 2) that form a statistically consistent relationship between biochemical activities and descriptors. The result shows that model 2 had better predictive ability than model 1 with an R2 value of 0.741, Q2(LOO) value of 0.648, and R2pred value of 0.608. The same group of compounds were also subjected to 3D-QSAR using CoMFA (ffdsel and uvepls) methodology. The CoMFA (uvepls) has reasonable R2, Q2(LOO), Q2(LTO), and Q2(LMO) values than CoMFA (ffdsel), suggesting that the model has excellent internal predictive power and good predictive capacity. The extracted contour maps

show the impact of steric and electrostatic fields on the type 1 diabetes inhibitory activity of the aligned molecules. Docking evaluation yields a qualitative representation of ligand (compound 17) and protein interactions, which can be compacted using CoMFA maps and the 2D-QSAR model. Both CoMFA and docking and molecular dynamics simulation studies show that the bulky group, electron donor, and electron acceptor are crucial for a potentially active ligand, and that the hydrogen-bonded interactions of the compound (compound 17) with amino acids of the target protein are also beneficial for type 1 diabetes inhibition.

Conflict of interest

The authors confirm that this article's content has no conflicts of interest.

Acknowledgments

The authors gratefully acknowledge the Department of Chemistry, Ahmadu Bello University, Zaria (Samaru, Zaria-Nigeria); for computational studies, and as part of the Ph.D. thesis.

References

[1] E. L. K. Khatabi, I. Aanouz, A. Khaldan, R. El-Mernissi, M. A. Ajana, M. Bouachrine, and T. Lakhlifi, Green and Applied Chemistry., 9, 16-29 (2020).

[2] E. I. Edache, A. Uzairu, P. A. Mamza, G. A. Shallangwa. *Biomed J Sci & Tech Res.*, 3426472-26489 (2021). DOI: 10.26717/BJSTR.2021.34.005509.

[3] A. Valadkhani, M. Asadollahi-Baboli and A. Mani-Varnosfaderani. *J. Braz. Chem. Soc.*, 26, 619-631, (2015). http://dx.doi.org/10.5935/0103-5053.20150017.

[4] U. B. Vitthal and Gawade, S. Pratapro, Pharmacophore., 7 , 342-348, (2016).

[5] N. A. Husna, A. Bustamam, A. Yanuar, D. Sarwinda, O. Hermansyah. AIP Conference Proceedings., 2264, 030010 (2020); https://doi.org/10.1063/5.0024161

[6] Y. Boukarai, F. Khalil, M. Bouachrine. *JMES.*, 8, 1533-1545, (2017).

[7] WHO. WHO Factsheets. http://wwwwhoint/mediacentre/factsheets/fs312/en/ 2015. Data Accessed From Official Diabetes Webpage of WHO.

[8] S. Wild, G. Roglic, A. Green, R. Sicree, H. King., 27,1047–1053 (2004).

[9] M. Javanbakht, H. R. Baradaran, A. Mashayekhi, A. A. Haghdoost, M. E. Khamseh, E. Kharazmi, A. Sadeghi. PLoS ONE 6(10): e26864 (2011). doi: 10.1371/journal.pone.0026864.

[10] E. I. Edache, A. Uzairu, P. A. Mamza and G. A. Shallangwa. *Chem. Rev. Lett vol.* 3 (Article in press). Doi: 10.22034/CRL.2021.254804.1088.

[11] E. I. Edache and S. Saidu. *African Journal of Biology and Medical Research.,* 3, 67-89 (2020).

[12] E. I. Edache, A. Uzairu, P. A. Mamza and G. A. Shallangwa. *A rational approach to antibacterial drug design.,* 4, 21-36, (2020). https://doi.org/10.31248/JDPS2020.036.

[13] E. I. Edache, A. Uzairu, P. A. Mamza and G. A. Shallangwa. *J. Chem. Lett.,* 1, 123-138 (2020). Doi: 10.22034/JCHEMLETT2021.262437.1011.

[14] O. Trott, A.J. Olson, *J Comput Chem.,* 31, 455– 461 (2010).

[15] W. Humphrey, A. Dalke, and K. Schulten, J. Mol. Graph., 14, 33–38 (1996).

[16] C. W. Yap, *J Comput Chem.,* 32, 1466-1474 (2011). http://padel.nus.edu.sg

[17] D. Ballabio, V. Consonni, A. Mauri, M. Claeys-Bruno, M. Sergent, R. Todeschin, *Chemometrics and Intelligent Laboratory Systems.,* 136, 147-154 (2014).

[18] N. Adhikari, Sk. A Amin, A. Saha, and T. Jha, *Chemistry Select.,* 2, 7888 – 7898 (2017). DOI: 10.1002/slct.201701330.

[19] P. Tosco, T. Balle, *J Comput Aided Mol Des.,* 25, 777–783 (2011). DOI 10.1007/s10822-011-9462-9.

[20] P. Tosco, T. Balle, *J. Mol.Model.,* 17, 201–208 (2011). http://dx.doi.org/10.1007/s00894-010-0684-x.

[21] B. D. Stadinski, R. Obst, and E. S. Huseby. *J Clin Invest.,*126, 2040–2042 (2016). doi:10.1172/JCI88165.

[22] W. Humphrey, A. Dalke, and K. Schulten, *J. Mol. Graph.,* 14, 33–38 (1996).

[23] J. C. Phillips, R. Braun, W. Wang, J. Gumbart, E. Tajkhorshid, E. Villa, C. Chipot, R. D. Skeel, L. Kale, and K. Schulten. *J Comp Chem.,* 26,1781–1802 (2005).

[24] A. D. MacKerell, D. Jr, Bashford, V. Bellott, R. L. Dunbrack, J. Jr, Evanseck, M. J. Field, S. Fischer, J. Gao, H. Guo, S. Ha, D. Joseph, Kuchnir L., et al. *J. Phys. Chem. B.,* 102, 3586–3616 (1998)

[25] E. I. Edache, A. Uzairu and S. E. Abechi. *J. Comput. Methods Mol. Des.,* 5 , 61-76 (2015).

[26] E. I. Edache, D. E. Arthur and U. Abdulfatai. *J. Chem. and Mater. Res.,* 6, 3–13 (2016).

[27] A. Golbraikh and A. Tropsha. *J. Mol. Graphics and Model.,* 20 , 269-276 (2002).

[28] E. Pourbasheer, S. Riahi, M. R. Ganjali, P. Norouzi. *Eur. J. Med. Chem.*. 44, 5023–5028 (2009).

[29] T. I. Netzeva, A.P. Worth, T. Aldenberg, R. Benigni, M. T. D. Cronin, P. Gramatica, J. S. Jaworska, S. Kahn, G. Klopman, C. A. Marchant, G. Myatt, N. Nikolova-Jeliazkova, G. Y. Patlewicz, R. Perkins, D. W. Roberts, T. W. Schultz, D. T. Stanton, J. J. M. Van De Sandt, W. Tong, G. Veith, C. Yang. *Altern. Lab. Anim.,* 33, 155–173 (2005).

[30] OECD, Guidance Document on the Validation of (Quantitative) Structure-Activity Relationships [(Q)SAR] Models, Organisation for Economic Co-Operation and Development, Paris, France (2007).

[31] E. I. Edache, A. Uzairu, P. A. P. Mamza and G. A. Shallengwa. *J Drug Design Discov Res.,* 1, 36-52 (2020).

How to Cite This Article

Emmanuel Israel Edache, Adamu Uzairu, Paul Andrew Mamzaand Gideon Adamu Shallangwa , “2D-QSAR, 3D-QSAR, molecular docking, and molecular dynamics simulations in the probe of novel type I diabetes treatment” International Journal of New Chemistry., 9 (4) 351-382 (2022). DOI: https://doi.org/10.22034/ijnc.2021.529335.1161.